Synthesis and Magnetic Characterization of $[Fe(\eta^5\text{-}C_9Me_7)_2]^{\bullet+}[A]^{\bullet-}$ (A = TCNE, TCNQ, DDQ). X-ray Structure of $[Fe(\eta^5\text{-}C_9Me_7)_2]^{\bullet+}[TCNQ]^{\bullet-}$

V. J. Murphy and D. O'Hare*

Inorganic Chemistry Laboratory, University of Oxford, South Parks Road, Oxford OX1 3QR, U.K.

Received September 1, 1993®

Addition of a solution of bis(η^5-heptamethylindenyl)iron(II) to solutions containing polycyano acceptor molecules (TCNE (tetracyanoethylene), TCNQ (7,7,8,8-tetracyano-*p*-quinodimethane), or DDQ (2,3-dichloro-5,6-dicyanobenzoquinone)) results in the formation of 1:1 charge-transfer salts with the general composition $[Fe(\eta\text{-}C_9Me_7)_2]^{\bullet+}[A]^{\bullet-}$ [A = TCNE, TCNQ, DDQ]. A single crystal X-ray structure determination has been performed for $[Fe(\eta\text{-}C_9Me_7)_2][TCNQ]$. This compound belongs to the monoclinic centrosymmetric space group $P2_1/n$ with a = 11.800(10) Å, b = 17.144(8) Å, c = 19.538(10) Å, β = 107.85(8)°, Z = 4, R = 0.063, and R_w = 0.078. The solid-state structure consists of linear chains of $D^+A^-D^+A^-$ alternating donor and acceptor ions. The cation adopts a partially eclipsed conformation with a rotation angle of 85° between the permethylindenyl rings. The iron C_5-ring centroid distance is 1.717(8) Å with an average Fe–C distance of 2.108(8) Å. Solid-state magnetic susceptibility data for $[Fe(\eta\text{-}C_9Me_7)_2][TCNE]$ and $[Fe(\eta\text{-}C_9Me_7)_2][DDQ]$ in the temperature region 5–150 K can be modeled by the Curie–Weiss law ($\chi_{mol} = C/T - \theta$) with C = 0.96 and 0.53 (emu K)/mol and θ = –0.3(2) and –4(1) K, respectively. In contrast, the high-temperature magnetic susceptibility for $[Fe(\eta\text{-}C_9Me_7)_2][TCNQ]$ can be fitted to the Curie–Weiss law in the temperature region 10–100 K with C = 0.85 (emu K)/mol and θ = 6(1) K. At 2 K, the magnetization saturated at a rate faster than that predicted by the Brillouin function for two $S = {}^1/_2$ independent spins; however, hysteresis effects were not observed. At 4 T, the magnetization saturates close to the expected value of 11 000 (emu G)/mol for two $S = {}^1/_2$ units. In the temperature range 6–40 K, the magnetic susceptibility can be fitted to the isotropic 1-D Heisenberg model with a small ferromagnetic exchange parameter J = 5.0 K. The EPR spectrum of a single crystal of $[Fe(\eta\text{-}C_9Me_7)_2][TCNE]$, oriented with the needle axis of the crystal aligned perpendicular to the applied field, exhibits a single transition at g = 2.03, attributable to the $g_\perp$ transition observed for the $[Fe(\eta\text{-}C_9Me_7)_2]^{\bullet+}$ radical cation. The EPR spectrum of a frozen solution of $[Fe(\eta\text{-}C_9Me_7)_2][DDQ]$ exhibits an axially symmetric pattern with $g_\parallel$ = 2.77 and $g_\perp$ = 2.06, attributable to the $[Fe(\eta\text{-}C_9Me_7)_2]^{\bullet+}$ radical cation. The lower g anisotropy (Δg = 0.71) compared to those reported for ferrocenium systems reflects the lower symmetry of the permethylindenyl ligand.

Introduction

In recent years there has been significant progress in the development of low-dimensional molecular solids exhibiting cooperative magnetic properties.[1,2] The charge-transfer salt $[Fe(\eta\text{-}C_5Me_5)_2][TCNE]$, with a T_c of 4.8 K, was the first reported example of a molecular material exhibiting bulk ferromagnetic properties.[3] This material possesses a linear chain structural motif containing both in and out of registry chains of alternating donor and acceptor molecules. The mean field model predicts that T_c is proportional to the exchange integral J and the spin S as $S[2S + 1]$,[4,5] and the replacement of $[Fe(\eta\text{-}C_5Me_5)_2]$ ($S = {}^1/_2$) with $[Mn(\eta\text{-}C_5Me_5)_2]$ (S = 1) leads to the formation of a molecular magnetic material with a T_c = 8.8 K.[6] Until recently it was widely considered that the nature of the spin–spin coupling in these compounds was best explained in terms of an extended version of McConnell's configurational interaction mechanism.[7] This predicts that ferromagnetic coupling can be stabilized by the configurational interaction of the wave function of a stable or virtual excited triplet state with the wave function of the triplet ground state. This mechanism presupposes a non-half-filled partially occupied degenerate ground state configuration for either the donor or the acceptor species. Thus $[Fe(\eta\text{-}C_5Me_5)_2]$ (cation ground state $^2E_{2g}$) and $[Mn(\eta\text{-}C_5Me_5)_2]$ (cation ground state $^3E_{2g}$ or $^3A_{2g}$) fulfill the electronic structure requirements of this model. However, the validity of this model has recently been called into question on several counts.[8] The experimental observation of ferromagnetic ordering in the charge-transfer salts $[Cr(C_6Me_6)_2]^+[TCNE]^-$ (cation ground state $^2A_{1g}$) and $[Cr(C_5Me_5)_2]^+[TCNQ]^-$ (cation ground state $^4A_{1g}$) contradicts the McConnell model, which predicts antiferromagnetic interactions for these compounds.[9,10] The authors explain these observations by invoking, in the case of $[Cr(C_6Me_6)_2]^+[TCNE]^-$, charge-transfer excitation from the next highest occupied molecular orbital in $[Cr(C_6Me_6)_2]^+$ (e_{2g}) and, in the case of $[Cr(C_5Me_5)_2]^+[TCNQ]^-$, charge-transfer excitation to the next lowest unoccupied molecular orbital in $TCNQ^-$. McConnell's mechanism would then be consistent with the experimental observations. In addition, a recent qualitative theoretical discussion by Kahn[8,11] implies that this mechanism is an oversimplification since it does

* Abstract published in *Advance ACS Abstracts*, March 15, 1994.

(1) Miller, J. S. *Extended Linear Chain Compounds*; Plenum: New York, 1982.
(2) Miller, J. S.; Epstein, A. J.; Reiff, W. M. *Chem. Rev.* **1988**, *88*, 201–220.
(3) Miller, J. S.; Calabrese, J. C.; Rommelmann, H.; Chittipeddi, S. R.; Zhang, J. H.; Reiff, W. M.; Epstein, A. J. *J. Am. Chem. Soc.* **1987**, *109*, 769–781.
(4) Carlin, R. L. *Magnetochemistry*; Springer-Verlag: Berlin, 1986.
(5) Dixon, D. A.; Suna, A.; Miller, J. S.; Epstein, A. J. In *NATO ARW Magnetic Molecular Materials*; Kahn, O., Gatteschi, D., Eds.; Kluwer: Dordrecht, The Netherlands, 1991; pp 171–190.
(6) Yee, G. T.; Manriquez, J. M.; Dixon, D. A.; Mclean, R. S.; Groski, D. M.; Flippen, R. B.; Narayan, K. S.; Epstein, A. J.; Miller, J. S. *Adv. Mater.* **1991**, *3*, 309–311.
(7) McConnell, H. M. *Proc. Robert A. Welch Found. Conf. Chem. Res.* **1967**, *11*, 144.
(8) Kollmar, C.; Kahn, O. *J. Am. Chem. Soc.* **1991**, *113*, 7987–7994.
(9) Miller, J. S.; O'Hare, D.; Chatraborty, A.; Epstein, A. J. *J. Am. Chem. Soc.* **1989**, *111*, 7853.
(10) Miller, J. S.; Mclean, R. S.; Vazquez, C.; Calabrese, J. C.; Zuo, F.; Epstein, A. J. *J. Mater. Chem.* **1993**, 3.
(11) Kollmar, C.; Couty, M.; Kahn, O. *J. Am. Chem. Soc.* **1991**, *113*, 7994–8005.

0020-1669/94/1333-1833$04.50/0

Scheme 1[a]

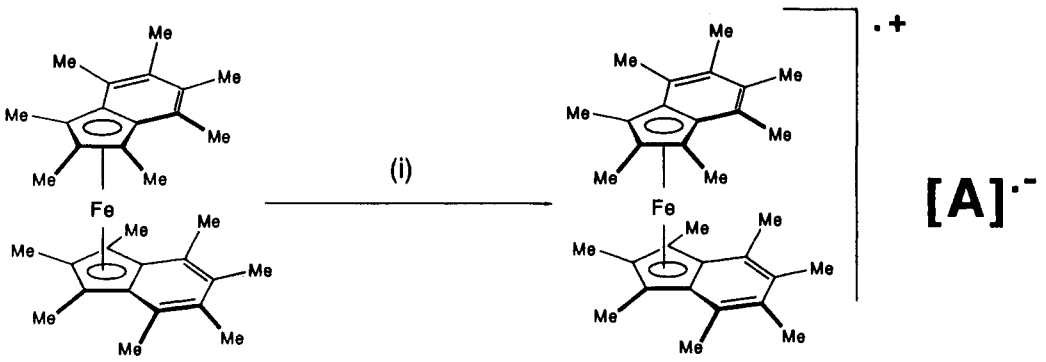

[a] (i) For **1**, TCNE in CH_3CN, yield 90%; for **2**, TCNQ in CH_2Cl_2, yield 90%; for **3**, DDQ in THF, yield 85%.

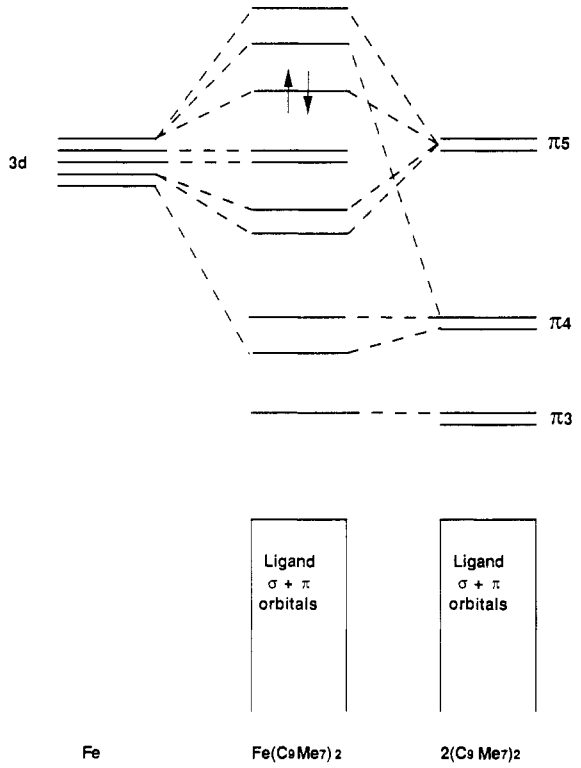

Figure 1. Qualitative molecular orbital scheme for $Fe(C_9Me_7)_2$.

not consider the full array of electronic configurations from the orbital pattern considered for this mechanism. The authors claim that its validity might be restricted to only special circumstances and then propose an alternative mechanism based upon a spin correlation effect upon the cyclopentadienyl rings.

In order to further test the validity of the McConnell mechanism, we have prepared charge-transfer salts incorporating the permethylindenyl ligand into the donor species (Scheme 1). The bonding in permethylindenyl compounds and the electron donating ability closely resemble those of the analogous pentamethylcyclopentadienyl compounds.[12,13] Figure 1 shows the qualitative molecular orbital diagram for $Fe(\eta\text{-}C_9Me_7)_2$ deduced from previous photoelectron spectroscopy studies.[14] The lower symmetry of the permethylindenyl ligand compared to the cyclopentadienyl ligand leads to a nondegenerate A_1 ground state configuration for $Fe(\eta\text{-}C_9Me_7)_2$, and magnetic studies in this report indicate a nondegenerate $^2A_1$ ground state configuration for the $[Fe(\eta\text{-}C_9Me_7)_2]^{\bullet+}$ radical cation. This ground state configuration is unable to support the stabilization of ferromagnetic coupling according to McConnell's model, which predicts antiferromagnetic behavior for these complexes. Here we report the synthesis and magnetic characterization of $[Fe(\eta\text{-}C_9Me_7)_2]^{\bullet+}$-$[A]^{\bullet-}$ (A = TCNE, TCNQ, DDQ) and show that the nondegenerate $^2A_1$ ground state configuration of the radical cation in these charge-transfer solids can indeed support ferromagnetic ordering at low temperatures.

Table 1. Crystallographic Details for $[Fe(\eta^5\text{-}C_9Me_7)_2][TCNQ]\cdot CH_2Cl_2$

chemical formula: $FeC_{44}H_{46}N_4CH_2Cl_2$	fw = 771.65
a = 11.800(10) Å	space group: $P2_1/n$ (14)
b = 17.144(8) Å	T = 23 °C
c = 19.538(10) Å	λ = 0.710 69 Å
β = 107.85(8)°	ρ_{obsd} = 1.36 g cm^{-3}, ρ_{calcd} = 1.38 g cm^{-3}
V = 3762 Å^3	μ = 5.8 cm^{-1}
Z = 4	$R^a(F_o)$ = 0.063, $R_w{}^b(F_o)$ = 0.078

[a] $R = \Sigma||F_o| - |F_c||/\Sigma|F_o|$. [b] $R_w = \{\Sigma(|F_o| - |F_c|)^2/\Sigma|F_o|^2\}^{1/2}$.

Experimental Section

General Procedures. All reactions were performed using standard Schlenk techniques or in a Vacuum Atmospheres dribox under a nitrogen atmosphere. Solvents were dried by refluxing over an appropriate drying agent in a continuous stream of nitrogen. Tetrahydrofuran and diethyl ether were refluxed over sodium potassium alloy, MeCN was refluxed over CaH_2, and CH_2Cl_2 was refluxed over P_2O_5. Solvents were distilled prior to use and stored over molecular sieves (type 4 Å) in flame-dried ampoules.

Synthesis. The syntheses of heptamethylindene and bis(η^5-heptamethylindenyl)iron(II) are described in detail elsewhere.[14]

$[Fe(\eta\text{-}C_9Me_7)_2][TCNE]$ (1). A solution of TCNE (26 mg, 0.208 mmol) in MeCN (20 cm^3) was added slowly to a solution of $Fe(\eta\text{-}C_9Me_7)_2$ (100 mg, 0.208 mmol) in MeCN (20 cm^3) at 50 °C with constant stirring. Upon cooling, a dark green precipitate was obtained which was collected by filtration. The resultant dark green solid was washed with diethyl ether and recrystallized from MeCN to produce dark green needlelike crystals of $[Fe(\eta\text{-}C_9Me_7)_2][TCNE]$ in 85% yield (108 mg, 0.177 mmol). Anal. Found (calcd) for $C_{38}H_{42}N_4Fe$: C, 74.45 (74.75); H, 6.91 (6.88); N, 8.97 (9.18).

$[Fe(\eta\text{-}C_9Me_7)_2][TCNQ]$ (2). A solution of TCNQ (42 mg, 0.208 mmol) in THF (80 cm^3) was added slowly to a solution of $Fe(C_9Me_7)_2$ (100 mg, 0.208 mmol) in THF (20 cm^3) with constant stirring. A dark green precipitate was immediately formed, collected by filtration, and washed with diethyl ether. The resultant dark green solid was recrystallized from CH_2Cl_2 to produce dark green crystals of $[Fe(\eta\text{-}C_9Me_7)_2][TCNQ]$ in 90% yield (128 mg, 0.187 mmol). Crystals for X-ray analysis were obtained by slow diffusion of diethyl ether into a CH_2Cl_2 solution. Anal. Found (calcd) for $C_{44}H_{46}N_4Fe\cdot CH_2Cl_2$: C, 69.67 (70.04); H, 6.70 (6.27); N, 7.01 (7.27).

(12) Cauletti, C.; Green, J.; Kelly, M. R.; Powell, P.; Tilborg, J. V.; Robbins, J.; Smart, J. *J. Electron Spectrosc. Relat. Phenom.* **1980**, *19*, 327–353.
(13) Crossley, N. S.; Green, J. C.; Nagy, A.; Stringer, G. *J. Chem. Soc., Dalton Trans.* **1989**, 2139.
(14) O'Hare, D.; Green, J. C.; Marder, T.; Collins, S.; Stringer, G.; Kakkar, A. K.; Kaltsoyannis, N.; Kuhn, A.; Lewis, R.; Mehnert, C.; Scott, P.; Kurmoo, M.; Pugh, S. *Organometallics* **1992**, *11*, 48–55.
(15) Day, P.; Kurmoo, M.; Mallah, T.; Marsden, I. R.; Frend, R. H.; Pratt, F. L.; Hayes, W.; Chasseau, D.; Gaultier, J.; Bravic, G.; Ducasse, L. *J. Am. Chem. Soc.* **1992**, *114*, 10722.

Table 2. Key Infrared Absorption Frequencies for Selected TCNE, TCNQ, and DDQ Compounds

	ν(C≡N), cm^{-1}	ν(C=O), cm^{-1}	ref
TCNE	2221 (m), 2259 (s)		9
$TCNE^{\bullet-}$	2144 (s), 2183 (s)		9
$TCNE^{2-}$	2069 (s), 2104 (s)		9
$[TCNE]_2^{2-}$	2159 (s), 2170 (s), 2189 (s)		9
$[Fe(C_9Me_7)_2][TCNE]$	2146 (s), 2185 (s)		this work
TCNQ	2222 (m), 2226 (m)		37
$TCNQ^-$	2153 (m), 2179 (s)		37
$TCNQ^{2-}$	2105 (s), 2150 (s)		37
$[TCNQ]_2^{2-}$	2182 (s), 2175 (s), 2156 (m)		31
$[Fe(C_9Me_7)_2][TCNQ]$	2150 (s), 2175 (s)		this work
DDQ	2234 (w), 2246 (w)	1691 (s), 1701 (s)	24
$DDQ^{\bullet-}$	2217 (s)	variable	24, 37
DDQ^{2-}	2187 (m), 2200 (s)	variable	24, 37
$[Co(C_5H_5)_2][DDQ]^a$	2220 (m)	1520, 1575[b]	24
$[Fe(C_9Me_7)_2][DDQ]$	2204 (s)	1524 (sh), 1542 (s), 1556 (s)	this work

[a] $[Co(C_5H_5)_2][DDQ]$ is reported to contain $[DDQ]_2^{2-}$ dimers in the solid state. [b] Relative intensities not reported. Intensities: s = strong, m = medium, w = weak, sh = shoulder peak.

$[Fe(\eta\text{-}C_9Me_7)_2][DDQ]$ (3). A solution of DDQ (140 mg, 0.620 mmol) in THF (25 cm^3) was added slowly to a solution of $Fe(C_9Me_7)_2$ (300 mg, 0.620 mmol) in THF (20 cm^3) with constant stirring. A dark red precipitate was immediately formed, collected by filtration, and washed with diethyl ether. The resultant dark red solid was recrystallized from CH_2Cl_2 to produce dark red crystals of $[Fe(\eta\text{-}C_9Me_7)_2][DDQ]$ in 90% yield (396 mg, 0.452 mmol). Anal. Found (calcd) for $C_{40}H_{42}N_2Cl_2O_2Fe$: C, 67.13 (67.70); H, 5.81 (5.97); N, 3.81 (3.96).

Physical Measurements. Infrared spectra were recorded on a Perkin Elmer 1710 Fourier transform spectrometer as Nujol mulls. The EPR spectra were obtained using an X-band Varian spectrometer and an Oxford Instruments cryostat. The samples were prepared under an atmosphere of nitrogen as microcrystalline solids, or as solutions, and recorded in 4-mm high-purity Spectrosil quartz tubes fitted with Young's Teflon stopcocks. Solid-state magnetic susceptibility measurements were carried out on microcrystalline samples. For **1**, susceptibility measurements were made using the Faraday method, and details for this are given elsewhere.[16] For **2** and **3**, measurements were made using a Cryogenics Consultants SCU500 superconducting quantum interference device (SQUID) susceptometer. The susceptibilities have been corrected for the intrinsic diamagnetism of the sample container and the diamagnetism of the electronic cores of the constituent atoms. Elemental microanalyses were performed by the analytical services section of the Inorganic Chemistry Laboratory.

X-ray Structure of $[Fe(\eta^5\text{-}C_9Me_7)_2][TCNQ]\cdot CH_2Cl_2$ ($2\cdot CH_2Cl_2$). The crystallographic data for this compound are given in Table 1. A dark green crystal of $2\cdot CH_2Cl_2$ was sealed under nitrogen in a Lindemann glass capillary and transferred to the goniometer head of an Enraf-Nonius CAD4 diffractometer interfaced to a PDP 11/23 minicomputer. Unit cell parameters were calculated from the setting angles of 25 carefully centered reflections. Three reflections were chosen as intensity standards and meausred every 3600 s of X-ray exposure time, and four orientation controls were measured every 200 reflections. The data were measured using graphite-monochromated Mo Kα radiation (λ = 0.710 69 Å) and an ω–2θ scan mode. There were no significant changes in the intensities of the standard reflections during the course of the data collection. A total of 4491 unique reflections were measured ($1.0° < \theta < 24°$) to give 2352 with $I \geq 3\sigma(I)$. The data were corrected for Lorentz and polarization effects and for the effects of absorption (based upon azimuthal scans for two reflections). The position of the iron atom was revealed by direct methods, and subsequent Fourier difference synthesis revealed the positions of all other non-hydrogen atoms. Refinement was performed using least squares techniques.[17-22] Corrections were made for the effects of anomalous dispersion and isotropic extinction during the final stages of the refinement.[19] Atomic scattering factors and anomalous dispersion coefficients were taken from ref 21. The indenyl ring carbon atoms were refined using isotropic thermal parameters due to the relatively low ratio of observations to least squares parameters. The asymmetric unit of $2\cdot CH_2Cl_2$ contains one CH_2Cl_2 molecule which is disordered over two sites related by an inversion through Cl(1). Least squares refinement revealed occupancy factors of 0.5 per site. Noncrystallographic chemical restraints were included in the least squares refinement in order to preserve the symmetry of the solvent molecule. A three-term Chebyshev weighting scheme was applied (coefficients: 10.2, 0.76, 8.04).[20] Final R and R_w values were 0.063 and 0.078, respectively.

Results and Discussion

Synthesis. The charge-transfer salts $[Fe(\eta\text{-}C_9Me_7)_2][TCNE]$, $[Fe(\eta\text{-}C_9Me_7)_2][TCNQ]$, and $[Fe(\eta\text{-}C_9Me_7)_2][DDQ]$ are prepared in a relatively straightforward manner through the simple addition of the donor and acceptor molecules in a suitable solvent (Scheme 1).

Vibrational Spectroscopy. The infrared ν(C≡N) stretching frequencies of polycyano acceptor molecules are particularly sensitive to the extent of reduction, due to the population of the out-of-plane antibonding π orbital (for $TCNE^-$ and $TCNQ^-$, the b_{3g} orbital; for DDQ^-, the b_1 orbital), causing a decrease in the bond order between the carbon and the nitrogen. Table 2 summarizes the ν(C≡N) and ν(C=O) stretching frequencies for TCNE, TCNQ, and DDQ in a variety of oxidation states, along with the observed stretching frequencies for $[Fe(\eta\text{-}C_9Me_7)_2][TCNE]$, $[Fe(\eta\text{-}C_9Me_7)_2][TCNQ]$, and $[Fe(\eta\text{-}C_9Me_7)_2][DDQ]$. These comparisons clearly indicate the presence of monoreduced isolated anions in the complexes $[Fe(\eta\text{-}C_9Me_7)_2][TCNE]$ and $[Fe(\eta\text{-}C_9Me_7)_2][TCNQ]$. X-ray studies performed on the dimeric dianions $[TCNE]_2^{2-}$ and $[TCNQ]_2^{2-}$ have revealed a lowering of the molecular symmetry due to an out-of-plane deformation.[23,7] This is consistent with the presence of three infrared active bands rather than two for the isolated monoanions. Thus the presence of diamagnetic dimeric dianions can be ruled out in the cases of $[Fe(\eta\text{-}C_9Me_7)_2][TCNE]$ and $[Fe(\eta\text{-}C_9Me_7)_2][TCNQ]$. The ν(C≡N) stretching frequency reported for $[Fe(\eta\text{-}C_9Me_7)_2][DDQ]$ is slightly red-shifted with respect to the corresponding frequencies reported for other DDQ, $DDQ^{\bullet-}$, and DDQ^{2-} complexes.[24] To our knowledge, there is very little infrared data reported for $[DDQ]_2^{2-}$ dimers, although

(16) O'Hare, D.; Lewis, R.; Kuhn, A.; Kurmoo, M. *Synth. Met.* **1991**, *41–43*, 1695.
(17) Caruthers, J.; Watkin, D. W. *CRYSTALS users manual*; Oxford University Computer Centre: Oxford, U.K., 1975.
(18) North, A. C. T.; Phillips, D. C.; Mathews, F. S. *Acta Crystallogr.* **1968**, *A24*, 351.
(19) Larsen, A. C. *Acta Crystallogr.* **1967**, *23*, 664.
(20) Caruthers, J.; Watkin, D. W. *Acta Crystallogr.* **1979**, *A35*, 698.
(21) *International Tables for X-Ray Crystallography*; Kynoch Press: Birmingham, AL, 1974; Vol. 4, p 9.
(22) Rollet, J. S. *Computing Methods in Crystallography*; Pergamon Press: Oxford, U.K., 1965.
(23) Miller, J. S.; Zhang, J. H.; Reiff, W. M.; Dixon, D. A.; Preston, L. D.; Reis, A. H., Jr.; Gebert, E.; Extine, M.; Troup, J.; Epstein, A. J.; Ward, M. D. *J. Phys. Chem.* **1987**, *91*, 4344–4360.
(24) Miller, J. S.; Krusic, P. J.; Dixon, D. A.; Reiff, W. M.; Zhang, J. H.; Anderson, E. C.; Epstein, A. J. *J. Am. Chem. Soc.* **1986**, *108*, 4459–4466.

Table 3. Fractional Atomic Coordinates, Isotropic Thermal Parameters, or Equivalent Isotropic Parameters[a] for $[Fe(\eta\text{-}C_9Me_7)_2][TCNQ]\cdot CH_2Cl_2$[b]

	x/a	y/b	z/c	U_{eq}/U_{iso}
Fe(1)	0.0126(1)	0.19637(6)	0.14491(6)	0.0305
C(1)	0.1738(7)	0.2625(4)	0.1704(4)	0.033(2)[c]
C(2)	0.1501(7)	0.2322(4)	0.2346(4)	0.034(2)[c]
C(3)	0.1491(7)	0.1503(5)	0.2301(4)	0.040(2)[c]
C(4)	0.1639(7)	0.1274(5)	0.1626(4)	0.041(2)[c]
C(5)	0.1840(6)	0.1976(5)	0.1265(4)	0.033(2)[c]
C(6)	0.2019(7)	0.2106(5)	0.0583(4)	0.039(2)[c]
C(7)	0.2096(7)	0.2855(5)	0.0373(4)	0.043(2)[c]
C(8)	0.1952(7)	0.3501(5)	0.0790(4)	0.045(2)[c]
C(9)	0.1784(7)	0.3404(5)	0.1458(4)	0.039(2)[c]
C(10)	0.1376(8)	0.2764(5)	0.2980(4)	0.0429
C(11)	0.1388(8)	0.0957(5)	0.2875(5)	0.0573
C(12)	0.1695(8)	0.0438(5)	0.1414(5)	0.0560
C(13)	0.2151(8)	0.1425(6)	0.0118(5)	0.0553
C(14)	0.2325(9)	0.3018(6)	−0.0338(5)	0.0620
C(15)	0.195(1)	0.4317(6)	0.0501(6)	0.0730
C(16)	0.1685(8)	0.4062(5)	0.1938(5)	0.0522
C(17)	−0.1448(7)	0.2676(4)	0.1142(4)	0.035(2)[c]
C(18)	−0.1220(7)	0.2289(4)	0.0553(4)	0.037(2)[c]
C(19)	−0.1274(8)	0.1478(5)	0.0635(4)	0.047(2)[c]
C(20)	−0.1426(7)	0.1334(5)	0.1324(4)	0.045(2)[c]
C(21)	−0.1584(6)	0.2073(4)	0.1626(4)	0.046(2)[c]
C(22)	−0.1764(7)	0.2284(4)	0.2298(4)	0.038(2)[c]
C(23)	−0.1778(7)	0.3065(5)	0.2457(4)	0.041(2)[c]
C(24)	−0.1621(8)	0.3650(5)	0.1983(5)	0.047(2)[c]
C(25)	−0.1483(7)	0.3477(5)	0.1317(4)	0.037(2)[c]
C(26)	−0.1045(8)	0.2664(5)	−0.0130(4)	0.0501
C(27)	−0.1202(9)	0.0866(6)	0.0090(6)	0.0594
C(28)	−0.1558(9)	0.0519(5)	0.1582(6)	0.0664
C(29)	−0.1898(8)	0.1643(6)	0.2807(5)	0.0559
C(30)	−0.1983(9)	0.3294(6)	0.3156(5)	0.0676
C(31)	−0.163(1)	0.4491(6)	0.2222(7)	0.0791
C(32)	−0.1375(9)	0.4075(5)	0.0794(5)	0.0583
C(33)	0.571(1)	0.2584(8)	−0.0252(6)	0.0662
C(34)	0.560(1)	0.1190(8)	−0.0222(6)	0.0728
C(35)	0.5552(8)	0.1898(7)	0.0122(5)	0.0581
C(36)	0.5530(7)	0.1958(6)	0.0806(5)	0.0523
C(37)	0.5138(8)	0.1309(6)	0.1170(5)	0.0490
C(38)	0.5289(9)	0.2711(6)	0.1111(5)	0.0588
C(39)	0.4925(8)	0.1384(6)	0.1826(5)	0.0595
C(40)	0.5063(8)	0.2784(5)	0.1754(5)	0.0492
C(41)	0.4888(7)	0.2120(5)	0.2137(5)	0.0431
C(42)	0.4715(8)	0.2204(5)	0.2822(5)	0.0504
C(43)	0.4663(8)	0.2951(6)	0.3121(5)	0.0519
C(44)	0.4579(8)	0.1548(7)	0.3225(5)	0.0577
C(45)	−0.0775(8)	−0.005(2)	0.4291(6)	0.078(7)[c]
N(1)	0.583(1)	0.3145(7)	−0.0531(5)	0.0933
N(2)	0.564(1)	0.0626(7)	−0.0518(6)	0.1145
N(3)	0.4632(8)	0.3554(6)	0.3366(5)	0.0755
N(4)	0.4522(8)	0.0994(6)	0.3556(5)	0.0803
Cl(1)	90	0	0.5	0.3855
Cl(2)	−0.023(1)	−0.0257(8)	0.3757(6)	0.2371

[a] $U_{eq} = 1/3[U_{11} + U_{22} + U_{33}]$. [b] Esd's are in parentheses. [c] Atoms refined using isotropic temperature factors.

Table 4. Selected Interatomic Distances (Å) for $[Fe(\eta^5\text{-}C_9Me_7)_2][TCNQ]\cdot CH_2Cl_2$[a]

Fe(1)–C(1)	2.137(7)	C(18)–C(19)	1.408(11)
Fe(1)–C(2)	2.082(8)	C(18)–C(26)	1.516(10)
Fe(1)–C(3)	2.084(8)	C(19)–C(20)	1.433(11)
Fe(1)–C(4)	2.080(8)	C(20)–C(21)	1.435(11)
Fe(1)–C(5)	2.160(7)	C(21)–C(22)	1.438(10)
Fe(1)–C(17)	2.148(8)	C(22)–C(23)	1.376(11)
Fe(1)–C(18)	2.072(8)	C(23)–C(24)	1.414(11)
Fe(1)–C(19)	2.084(9)	C(24)–C(25)	1.392(11)
Fe(1)–C(20)	2.074(8)	C(33)–N(1)	1.139(14)
Fe(1)–C(21)	2.157(7)	C(34)–N(2)	1.134(13)
C(1)–C(2)	1.462(10)	C(33)–C(35)	1.426(16)
C(1)–C(5)	1.431(10)	C(34)–C(35)	1.398(14)
C(1)–C(9)	1.426(10)	C(35)–C(36)	1.442(12)
C(2)–C(3)	1.406(10)	C(36)–C(37)	1.376(13)
C(3)–C(4)	1.437(10)	C(36)–C(38)	1.430(13)
C(4)–C(5)	1.450(10)	C(37)–C(39)	1.387(13)
C(5)–C(6)	1.430(10)	C(38)–C(40)	1.367(11)
C(6)–C(7)	1.360(10)	C(39)–C(41)	1.406(12)
C(7)–C(8)	1.415(11)	C(40)–C(41)	1.411(12)
C(8)–C(9)	1.390(10)	C(41)–C(42)	1.423(11)
C(17)–C(18)	1.457(10)	C(42)–C(43)	1.417(13)
C(17)–C(21)	1.419(11)	C(42)–C(44)	1.411(14)
C(43)–N(3)	1.143(12)	C(44)–N()4)	1.162(12)

[a] Esd's are in parentheses.

Table 5. Selected Bond Angles (deg) for $[Fe(\eta^5\text{-}C_9Me_7)_2][TCNQ]\cdot CH_2Cl_2$[a]

C(5)–C(1)–C(2)	108.1(6)	C(21)–C(17)–C(18)	107.2(6)
C(1)–C(2)–C(3)	107.5(7)	C(17)–C(18)–C(19)	107.8(7)
C(2)–C(3)–C(4)	109.3(7)	C(18)–C(19)–C(20)	109.1(7)
C(3)–C(4)–C(5)	107.6(7)	C(19)–C(20)–C(21)	107.7(7)
C(4)–C(5)–C(1)	107.3(6)	C(20)–C(21)–C(17)	107.9(6)
C(1)–C(5)–C(6)	120.1(7)	C(17)–C(21)–C(22)	119.7(7)
C(5)–C(6)–C(7)	118.1(7)	C(21)–C(22)–C(23)	117.8(7)
C(6)–C(7)–C(8)	122.3(6)	C(22)–C(23)–C(24)	121.9(7)
C(7)–C(8)–C(9)	121.6(8)	C(23)–C(24)–C(25)	122.5(8)
C(8)–C(9)–C(1)	117.3(7)	C(24)–C(25)–C(17)	116.9(7)
C(9)–C(1)–C(5)	120.5(7)	C(25)–C(17)–C(21)	121.4(7)
C(34)–C(35)–N(2)	178.2(14)	C(35)–C(33)–N(1)	177.7(12)
C(34)–C(35)–C(36)	123.7(11)	C(33)–C(35)–C(36)	120.4(10)
C(35)–C(36)–C(37)	121.8(10)	C(35)–C(36)–C(38)	119.4(10)
C(36)–C(37)–C(39)	120.5(9)	C(36)–C(38)–C(40)	120.4(9)
C(37)–C(39)–C(41)	121.4(9)	C(38)–C(40)–C(41)	121.0(9)
C(39)–C(41)–C(42)	122.0(8)	C(40)–C(41)–C(42)	120.2(8)
C(41)–C(42)–C(43)	121.1(8)	C(41)–C(42)–C(44)	121.2(9)
C(42)–C(43)–N(3)	179.3(10)	C(42)–C(44)–N(4)	176.6(11)

[a] Esd's are in parenthesis.

their existence has been confirmed crystallographically.[25,26] The infrared data reported for $[Co(\eta\text{-}C_5H_2)_2][DDQ]$, a complex thought to contain $[DDQ]_2^{2-}$ dianions in the solid state, contrast with the data reported here. The $\nu(C{\equiv}N)$ band reported for $[Co(\eta\text{-}C_5H_2)_2][DDQ]$ displays a slight blue shift with respect to the corresponding band in $[Co(\eta\text{-}C_5Me_2)_2][DDQ]$ (containing isolated $DDQ^{\bullet-}$ anions).[24] $\nu(C{=}O)$ stretching frequencies for DDQ molecules decrease significantly upon reduction in accordance with a decrease in the C–O bond order from one in DDQ to two in DDQ^{2-}. However, values reported for $DDQ^{\bullet-}$ complexes appear to be quite variable. For instance, $[Fe(\eta\text{-}C_5Me_5)_2][DDQ]$ (containing $S = 1/2$ donor and acceptor ions) has transitions reported at 1562 and 1544 cm^{-1}, while for $[N(Et)_4][DDQ]$, the transitions are reported at 1580 and 1538 cm^{-1}. Transitions at similar frequencies have been reported for $[Co(\eta\text{-}C_5H_5)_2][DDQ]$.[24,35] For $[Fe(\eta\text{-}C_9Me_7)_2][DDQ]$, we observed three bands in this region. It is therefore not possible to unambiguously assign the oxidation state of the DDQ counterion in the charge-transfer complex $[Fe(\eta\text{-}C_9Me_7)_2][DDQ]$ from the infrared data alone.

Structural Features of $[Fe(\eta\text{-}C_9Me_7)_2][TCNQ]\cdot CH_2Cl_2$ ($2\cdot CH_2Cl_2$). Fractional atomic coordinates, interatomic distances, and angles for compounds $2\cdot CH_2Cl_2$ and **2** are given in Tables 3–5. Figure 2 shows the molecular structure of compound $2\cdot CH_2Cl_2$ together with the atomic labeling scheme.

The $[Fe(\eta\text{-}C_9Me_7)_2]^{\bullet+}$ Radical Cation. The indenyl rotation angle (ra) has recently been defined as the angle formed by the intersection of the two lines determined by the centroids of the five- and six-membered rings.[27] Several other parameters have been defined to estimate the degree of distortion in indenyl complexes.[27,28] The slip parameter ($\Delta_{M\text{-}C}$) is defined as the difference in the average bond lengths of the metal to the ring-

(25) Zanotti, G.; Del Pra, A.; Bozio, R. *Acta Crystallogr.* **1982**, *B38*, 1225–1229.
(26) Mayerle, J. J.; Torrance, J. B. *Bull. Chem. Soc. Jpn.* **1981**, *54*, 3170–3172.
(27) O'Hare, D.; Murphy, V. J.; Kaltsoyannis, N. *J. Chem. Soc., Dalton Trans.* **1993**, 383–392.
(28) Westcott, S. A.; Kakkar, A. K.; Stringer, G.; Taylor, N. J. *J. Organomet. Chem.* **1990**, *394*, 777–794.

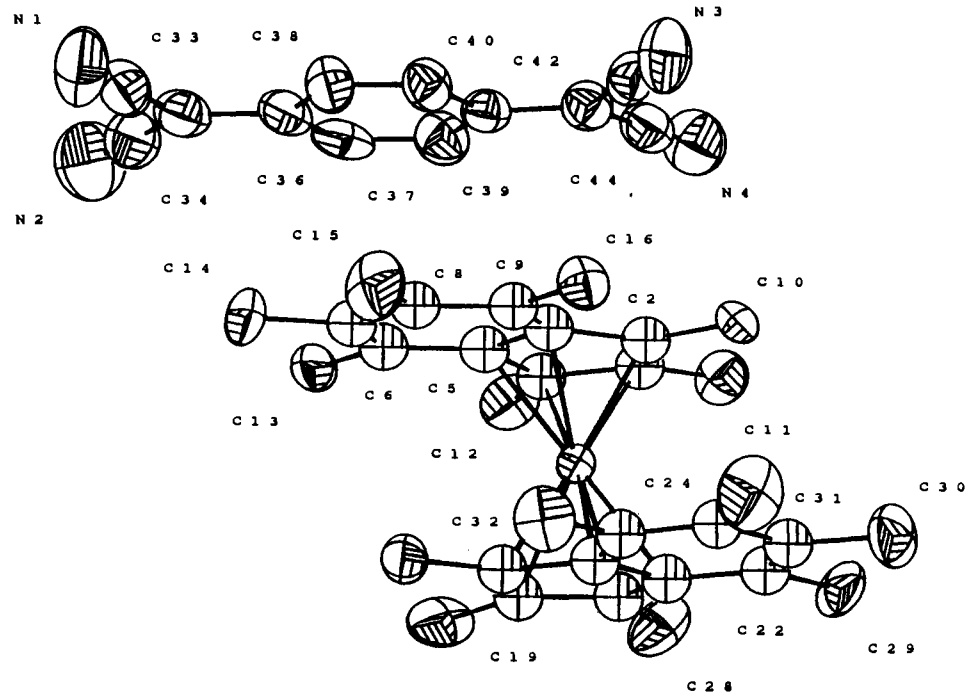

Figure 2. Molecular structure together with atomic labeling for $[Fe(C_9Me_7)_2][TCNQ]\cdot CH_2Cl_2$. Atoms are displayed with 50% ellipsoids; the solvent molecule and hydrogen atoms have been omitted for clarity.

Table 6. Structural Parameters for the $[Fe(\eta^5\text{-}C_9Me_7)_2]^{\bullet+}$ Radical Cation

M–C (av)	2.108(8) Å
Δ_{M-C}	0.067, 0.076 Å
M–C_5 (centroid) (av)	1.717(8) Å
ha	3.0°, 3.9°
fa	1.5°, 1.4°
ra	85°

junction carbons C(1), C(5) and the metal to adjacent carbon atoms of the five-membered ring, C(2), C(4). The hinge angle (ha) is defined as the angle between the planes defined by [C(2), C(3), C(4)] and [C(1), C(2), C(3), C(4), C(5)]. The fold angle (fa) is defined as the angle between the planes defined by [C(2), C(3), C(4)] and [C(1), C(5), C(6), C(7), C(8), C(9)]. Hence ha represents bending at C(2), C(4) and fa represents bending at C(1), C(5).

Table 6 reports Δ_{M-C}, ra, fa, ha, and M–C_5(centroid) values for the $[Fe(\eta^5\text{-}C_9Me_7)_2]^{\bullet+}$ radical cation. The values of Δ_{M-C}, fa, and ha suggest almost undistorted η^5-coordination of the permethylindenyl rings, consistent with the values observed for $[Fe(\eta^5\text{-}C_9Me_7)_2]$, $[Fe(\eta^5\text{-}C_9H_7)_2]$,[28] and $[Fe(\eta^5\text{-}C_9Me_2H_7)_2]^{\bullet+}$.[29] The rotation angle of 85° infers a partially eclipsed conformation, consistent with ra values reported for other permethylindenyl radical cations.[27] Figure 3 shows the structure of the $[Fe(\eta^5\text{-}C_9Me_7)_2]^{\bullet+}$ radical cation viewed orthogonal to the plane of the permethylindenyl rings; the partially eclipsed geometry can be clearly seen. The Fe–C distances range between 2.074(8) and 2.157(7) Å, and these values are slightly longer than those observed for $[Fe(\eta^5\text{-}C_9Me_7)_2]$; this trend has already been noted for $[Fe(\eta^5\text{-}C_5H_5)_2]/[Fe(\eta^5\text{-}C_5H_5)_2]^{\bullet+}$ and $[Fe(\eta^5\text{-}C_5Me_5)_2]/[Fe(\eta^5\text{-}C_5Me_5)_2]^{\bullet+}$.[3,30]

The $TCNQ^-$ Anion. The bond lengths and angles shown in Table 5 are consistent with those reported for other singly reduced $TCNQ^-$ monoanions.[31,32] The planes of the $TCNQ^-$ anions and the permethylindenyl rings are essentially parallel with a small dihedral angle of 1°. The distance between these planes is 3.50 Å, and the distance between the least squares plane of the anion and the iron atom is 5.22 Å. These values are very similar to those reported for $[Fe(\eta^5\text{-}C_5Me_5)_2][TCNQ]$[32] and $[Fe(\eta^5\text{-}C_5Me_5)_2][TCNE]$.[3]

Solid-State Structure. Similar to other reported organometallic charge-transfer salts, the structure of **2**·CH_2Cl_2 consists of parallel, 1-D chains of alternating radical cations and anions, stacked along a crystallographic axis.[32,3] The intrachain Fe–Fe separation is 11.800 Å, significantly longer (ca. 1.3 Å) than those reported for the ferromagnet $[Fe(\eta^5\text{-}C_5Me_5)_2][TCNE]$[3] and the metamagnet $[Fe(\eta^5\text{-}C_5Me_5)_2][TCNQ]$.[32] The unit cell of **2**·CH_2Cl_2 contains four distinct $D^+A^-D^+A^-$ units and three unique interchain arrangements. Chains I–III and I–IV are out of registry whereas chains I and II are essentially in registry. These interchain arrangements are presented in Figures 4, 5, and 6 along with shortest Fe···Fe separations. The shortest interchain Fe–Fe distances for both in and out of registry chains are again significantly longer than those reported for $[Fe(\eta\text{-}C_5Me_5)_2]$-[TCNE] and $[Fe(\eta\text{-}C_5Me_5)_2][TCNQ]$. In view of this comparative structural information, it might be reasonable to anticipate weaker spin–spin interactions for compound **2**·CH_2Cl_2.

EPR Measurements. The EPR spectrum of a frozen CH_2Cl_2 solution of $[Fe(\eta\text{-}C_9Me_7)_2]^{\bullet+}[PF_6]$, reported elsewhere, exhibits an axially symmetric pattern characterized by $g_\parallel = 2.93$ and $g_\perp = 2.15$.[14] The lower g-tensor anisotropy $\Delta g = 0.78$ compared to ferrocenium systems reflects the inherently lower symmetry of the permethylindenyl system.[33,34] Variable-temperature (4–300 K) measurements were performed on a single crystal of **1**, with the needle axis of the crystal aligned perpendicular to the magnetic field. The spectra are dominated by the presence of a single transition at $g = 2.03$. The shape and position of the signal are similar to those observed for the $g_\perp$ transition of $[Fe(\eta\text{-}C_9Me_7)_2]^{\bullet+}$-$[PF_6]^-$. Although the infrared data suggest the presence of isolated monoreduced anions, we did not observe another resonance which could be attributed to the $TCNE^-$ moiety. The plot of the

(29) Treichel, P. M.; Johnson, J. W.; Calabrese, J. C. *J. Organomet. Chem.* **1975**, *88*, 215–225.
(30) Sullivan, B. W.; Foxman, B. *Organometallics* **1983**, *2*, 187–189.
(31) O'Hare, D.; Ward, M. D.; Miller, J. S. *Chem. Mater.* **1990**, *2* (6), 758.
(32) Miller, J. S.; Reiss, A. H.; Gebert, E.; Ritsko, J. J.; Salaneck, W. R.; Kovnat, L.; Cape, T. W.; Duyne, R. P. V. *J. Am. Chem. Soc.* **1979**, *101*, 7111–7113.
(33) Ammeter, J. H. *J. Magn. Reson.* **1978**, *30*, 299–325.
(34) Miller, J. S.; Glatzhofer, D. T.; O'Hare, D.; Reiff, W. M.; Chakraborty, A.; Epstein, A. J. *Inorg. Chem.* **1989**, *28*, 2930.

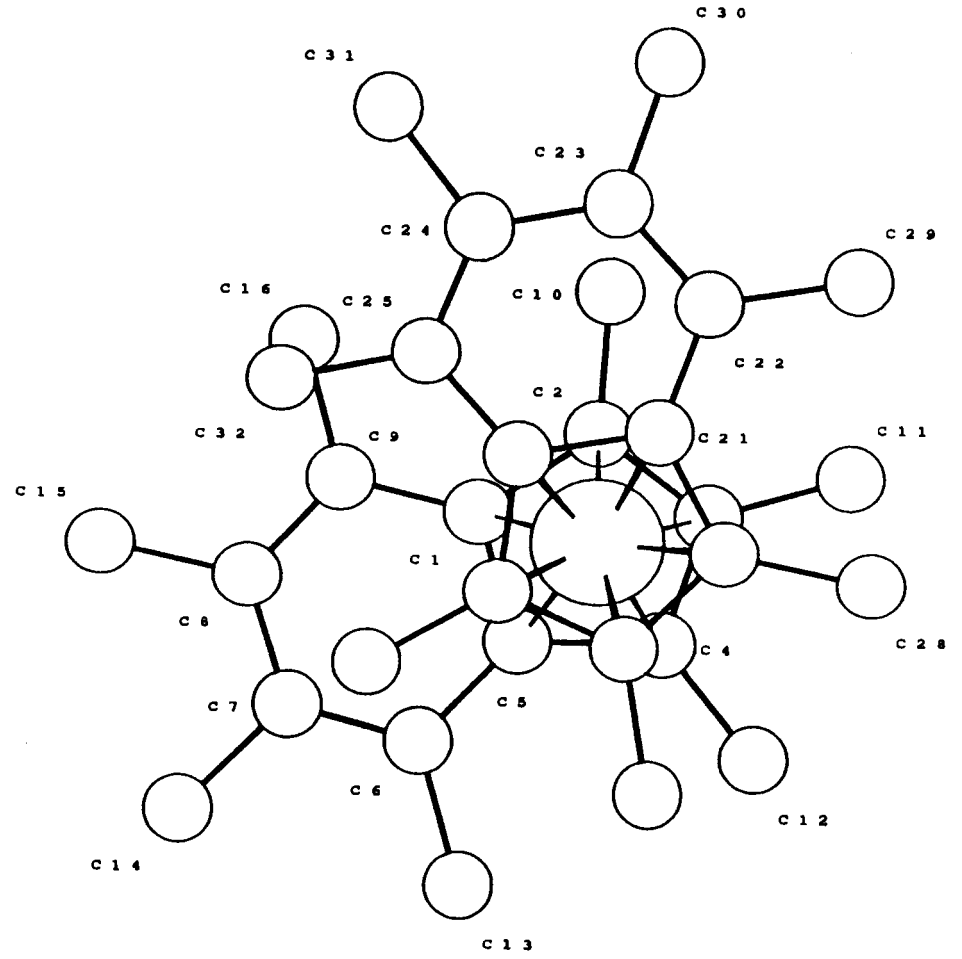

Figure 3. Molecular structure of $[Fe(C_9Me_7)_2][TCNQ]\cdot CH_2Cl_2$ showing the donor molecule only, with atomic labeling, viewed orthogonal to the permethylindenyl rings. Hydrogen atoms have been omitted for clarity.

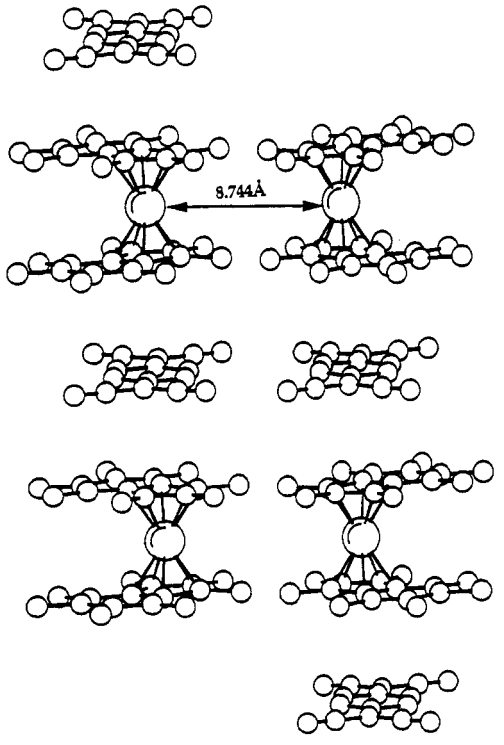

Figure 4. Out of registry chains I–III with illustrated Fe–Fe distances. The solvent molecule and hydrogen atoms have been omitted for clarity.

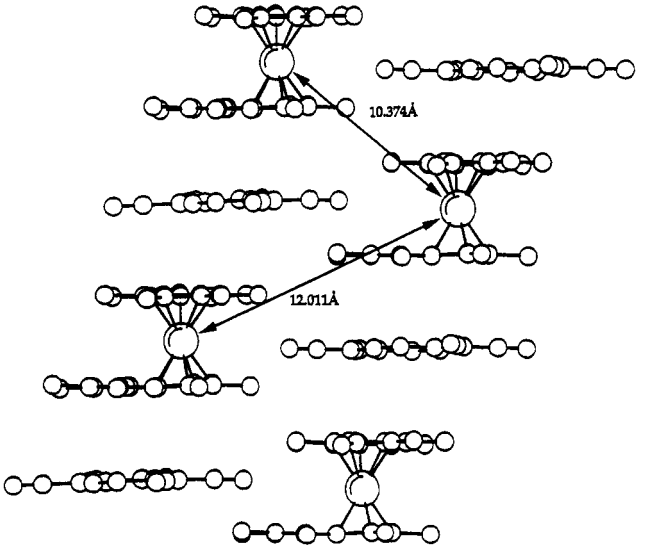

Figure 5. Out of registry chains I–IV with illustrated Fe–Fe distances. The solvent molecule and hydrogen atoms have been omitted for clarity.

reciprocal integrated intensity versus temperature (4.3–100 K) is shown in Figure 7. Regretably, we observed significant scattering of the data points due to temperature instability; however, the data does indicate a linear dependence ($I \alpha C/T - \theta$) with a small intercept ($\theta = 1 \pm 4$ K), indicating no spin–spin interactions for compound **1**.[15] The EPR spectrum of a frozen CH_2Cl_2 solution of compound **3** at 100 K can be seen in Figure 8. This spectrum is very similar to that observed for $[Fe(\eta\text{-}C_9Me_7)_2]^{\bullet+}[PF_6]^-$ with $g_\parallel = 2.77$ and $g_\perp = 2.06$. There was no signal attributable to the anion consistent with strong antiferromagnetic exchange between the $[DDQ]_2^{2-}$ dimers. There was

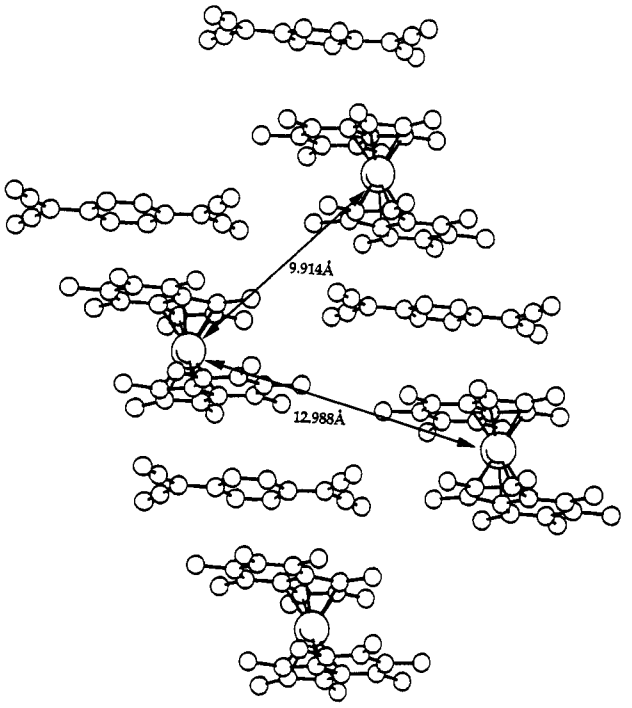

Figure 6. Out of registry chains II and III with illustrated Fe–Fe distances. The solvent molecule and hydrogen atoms have been omitted for clarity.

no evidence for a singlet–triplet transition between 4.3 and 290 K, indicating that the triplet state is not thermally accessible in this complex, in contrast to $[Co(\eta\text{-}C_5H_5)_2][DDQ]$.[24] No signal was observed for CH_2Cl_2 solutions and microcrystalline solids of compound **2** over the temperature range 4.3–300 K.

Magnetic Measurements. The magnetic susceptibility of a microcrystalline sample of **1** was measured over the temperature range 4–100 K using the Faraday method. The susceptibilities obey the Curie–Weiss expression, $\chi_{mol} = C/(T - \theta)$, with C = 0.96 (emu K)/mol and a small negative value of $\theta = -0.3(2)$ K. The observed effective moment ($\mu_{eff} = 2.77\mu_B$) is very close to the spin-only value expected for two noninteracting $S = {}^1/_2$ ions. These data are entirely consistent with the EPR data and indicate that, in contrast to the bulk ferromagnet $[Fe(\eta\text{-}C_5Me_5)_2]$-[TCNE],[3] compound **1** is a simple paramagnet with no long-range spin interactions. The $^2A_1$ HOMO for the $[Fe(\eta\text{-}C_9Me_7)_2]^{\bullet+}$ radical cation does not support the stabilization of ferromagnetic coupling in **1**. However, the absence of structural information precludes a discussion of magnetic models in relation to this compound. The magnetic susceptibility of a microcrystalline sample of compound **2** was initially measured over the temperature range 5–290 K using a SQUID device. The temperature dependence of the effective moment for **2** is shown in Figure 9. The high-temperature moment of 2.61 μ_B is very close to the spin-only value for two noninteracting $S = {}^1/_2$ molecules. At low temperatures the effective moment increases substantially, indicating ferromagnetic interactions. The reciprocal molar susceptibility is plotted as a function of temperature in Figure 10 with the low-temperature data inset. Above 15 K this complex obeys the Curie–Weiss expression with C = 0.85 (emu K)/mol and $\theta = 6(1)$ K, indicating significant ferromagnetic interactions. Below 15 K the susceptibilities deviate from the Curie–Weiss law and at 2 K exhibit a substantial field dependence. Figure 11 displays the magnetization versus field plots at 2, 4.5, and 10 K. At 2 K the magnetization data clearly show a marked deviation from a linear field dependence. Figure 12 demonstrates the low-temperature field dependence of the magnetization by comparison with the Brillouin function, which models the behavior of independent spins. The magnetization (M) for a noninteracting system is given by

$$M = NgSB_s(y) \quad \text{with} \quad y = g\mu_B SH/kT$$

where $B_s(y)$ is the Brillouin function defined by

$$B_s(y) = \frac{2S+1}{2S}\coth\left(\frac{2S+1}{2S}y\right) - \frac{1}{2S}\coth\left(\frac{1}{2S}y\right)$$

Figure 12 demonstrates that the increase of M versus H is faster than the Brillouin function, indicating a ferromagnetic interaction. The saturation magnetization is close to the theoretical value of 11 000 (emu G)/mol predicted for two g = 2.0 and $S = {}^1/_2$ units by the following equation:

$$M_s = NS\mu_B\sum g_i$$

However, no hysteresis effects were observed, which suggests that the data may be consistent with either a soft 3-D ferromagnet or lower dimensional magnetic ordering. The temperature dependence of the product of susceptibility and temperature can be modeled by a series expansion[35] for the 1-D Heisenberg model with ferromagnetic exchange:

$$\frac{\chi T}{Ng^2\mu_B{}^2} = [(1 + 5.80K + 16.90K^2 + 29.38K^3 + 29.83K^4 + 14.04K^5)/(1 + 2.80K + 7.01K^2 + 8.65K^3 + 4.47K^4)]^{2/3} \quad (1)$$

where $K = J/2kT$. A good fit of χT in equation 1 is obtained with a small interaction parameter J = 5.0 K (Figure 13). This value is significantly lower than the values quoted from single crystal studies performed on $[Fe(\eta\text{-}C_5Me_5)_2][TCNE]$ ($J_{intrachain} \approx 27$ K, $J_{interchain} \approx 8$ K, $T > 16$ K)[3,36] and may be indicative of the longer intrachain separations. The magnetic data characterizes **2**·CH_2Cl_2 as a 1-D Heissenberg ferromagnet at 2 K. McConnell's configurational interaction model cannot provide an explanation for the nature of the spin–spin coupling in this compound. The magnetic susceptibilities of compound **3** were measured over the temperature range 5–290 K, using a SQUID device. Figure 14 indicates that the susceptibilities can be modeled by the Curie–Weiss expression, with C = 0.53 (emu K)/mol and $\theta = -4(1)$ K. The observed value of the effective moment ($\mu_{eff} = 2.05\mu_B$, 5 K < T < 290 K) is very close to the spin-only value expected for the $S = {}^1/_2$ $[Fe(C_9Me_7)_2]^{\bullet+}$ cation ($\langle g\rangle$ = 2.3). This is entirely consistent with the EPR measurements which indicate a solid state structure containing $[DDQ]_2{}^{2-}$ dimers with a singlet ground state.

Conclusions

The charge-transfer salt $[Fe(C_9Me_7)_2][TCNE]$ has been characterized as a simple Curie–Weiss paramagnet between 4.2 and 100 K. The infrared data indicate the presence of isolated $TCNE^{\bullet-}$ anions, and we therefore propose that this compound has a ...$D^{\bullet+}A^{\bullet-}D^{\bullet+}A^{\bullet-}$... linear chain structural motif. The HOMO in the neutral complex $Fe(C_9Me_7)_2$ has been assigned as an A_1 orbital from previous photoelectron spectroscopy studies; this is consistent with the magnetic measurements performed on $[Fe(C_9Me_7)_2][PF_6]$ and compounds **1**–**3** which suggest a $^2A_1$

(35) Baker, G. A.; Rushbrooke, G. S.; Gilbert, H. E. *Phys. Rev.* **1964**, *135*, 1272–1277.
(36) Epstein, A. J.; Miller, J. S. In *Magnetic Molecular Materials*; Gatteschi, D., Ed.; Klewer: The Netherlands, 1991; p 159–169.
(37) Miller, J. S.; Dixon, D. A. *Science* **1987**, *235*, 871.

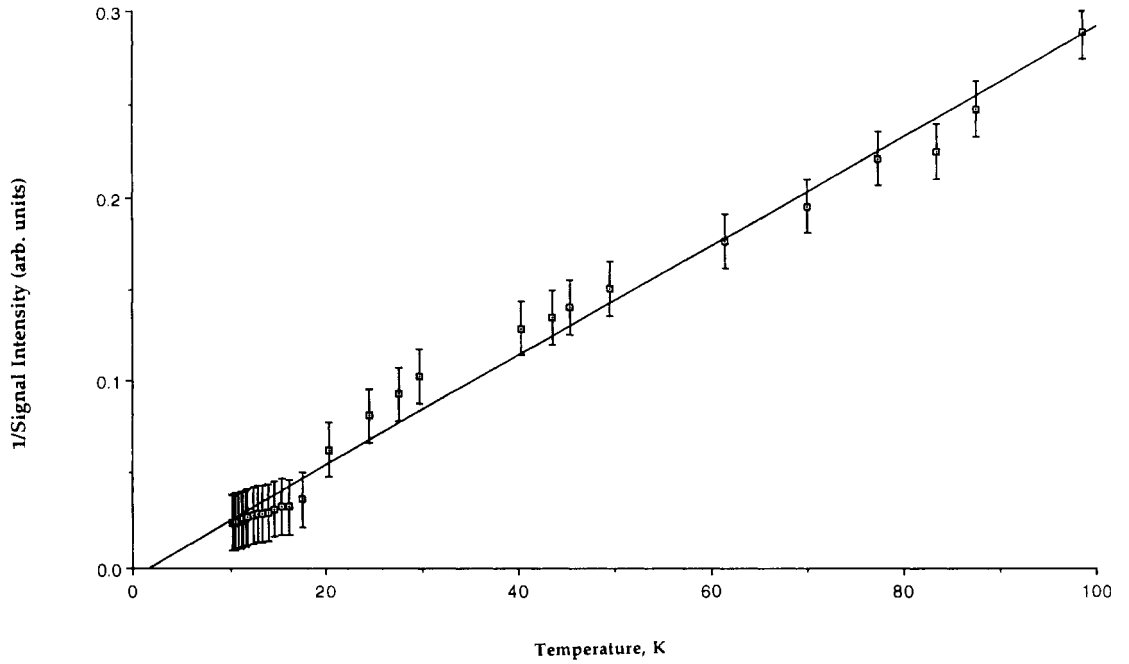

Figure 7. Plot of reciprocal integrated ESR intensity against temperature for $[Fe(C_9Me_7)_2][TCNE]$.

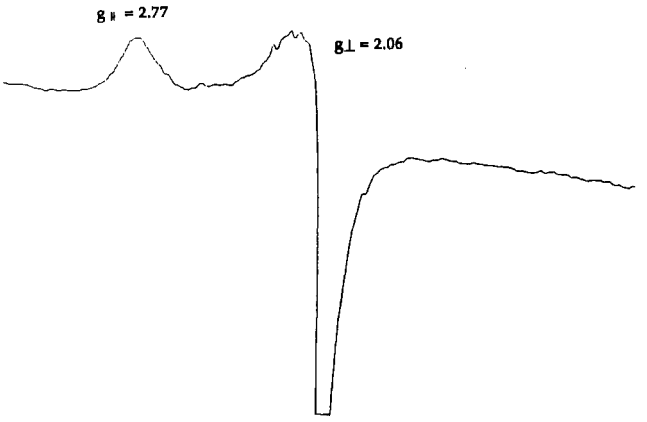

Figure 8. Axially symmetrical ESR pattern, performed at 100 K, for $[Fe(C_9Me_7)_2][DDQ]$.

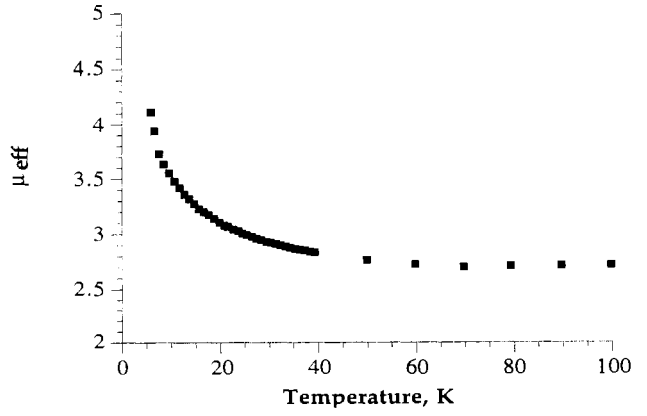

Figure 9. The temperature dependence of the effective moment for $[Fe(C_9Me_7)_2][TCNQ]$.

ground state configuration for the $[Fe(C_9Me_7)_2]^{\bullet+}$ radical cation. Thus the absence of magnetic ordering in **1** would appear to be consistent with McConnell's configurational interaction model which suggests that the A_1 ground state configuration cannot support the stabilization of ferromagnetic coupling with any of the counterions used in this study. However, the absence of structural information prevents a discussion of intra- and

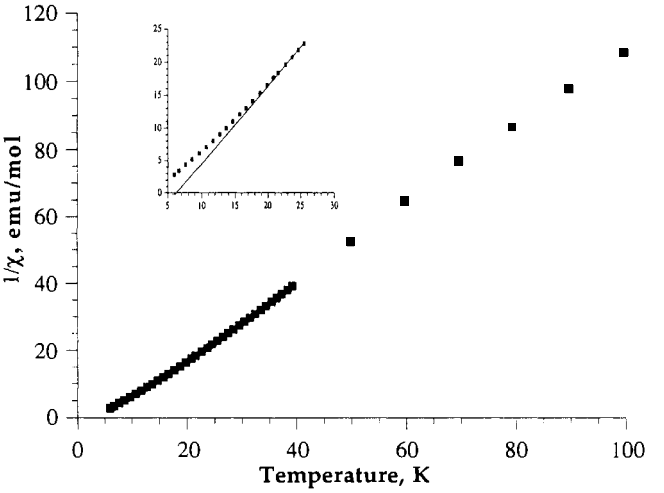

Figure 10. Plot of inverse molar susceptibility versus temperature for $[Fe(C_9Me_7)_2][TCNQ]$ with the low-temperature data inset.

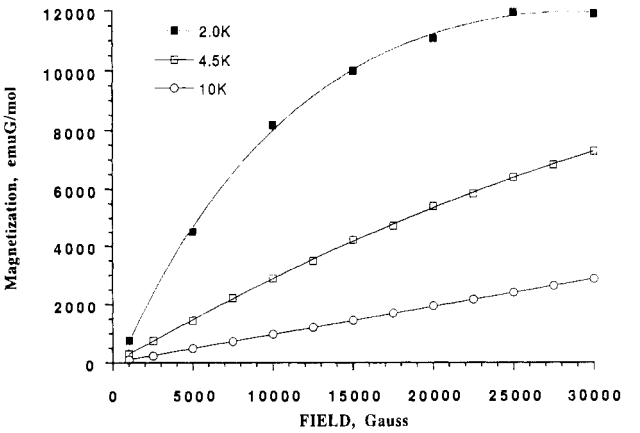

Figure 11. Field dependence of the magnetization for $[Fe(C_9Me_7)_2][TCNQ]$, at three different temperature values. The solid lines represent interpolation of the data points.

interchain arrangements and interatomic separations for comparison with the bulk ferromagnet $[Fe(C_5Me_5)_2][TCNE]$ and a discussion of the suitability of **1** for application to the McConnell

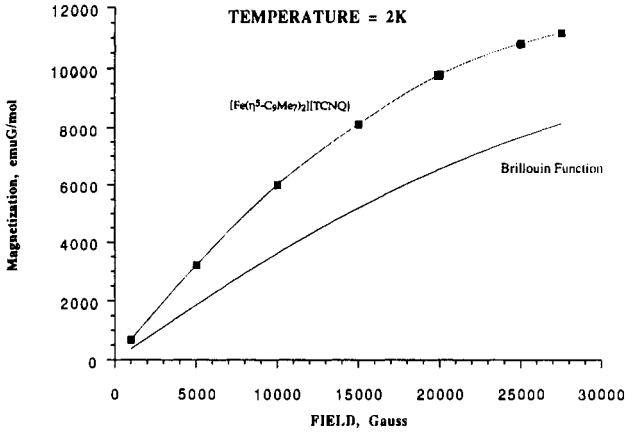

Figure 12. Magnetization as a function of the applied field for $[Fe(C_9Me_7)_2][TCNQ]$, performed at 2 K, compared to the Brillouin function. The solid line through the experimental plot represents interpolation of the data points.

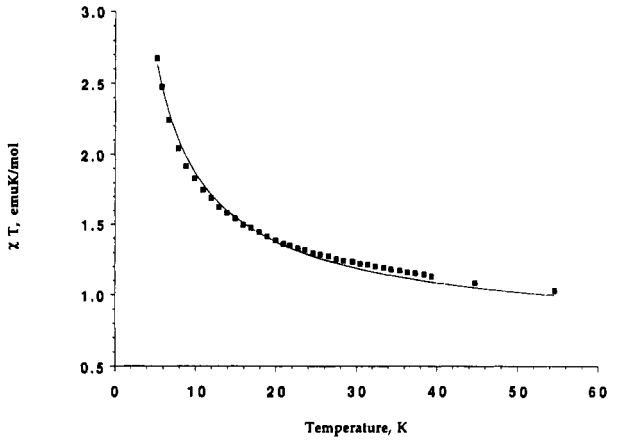

Figure 13. Plot of χT versus T for $[Fe(C_9Me_7)_2][TCNQ]$ compared to the isotropic Heisenberg model with ferromagnetic exchange. The solid line corresponds to values calculated according to the theoretical model with $S = {}^1/_2$ and $J = 5$ K.

model. The charge-transfer salt $[Fe(C_9Me_7)_2][DDQ]$ also behaves as a simple Curie–Weiss paramagnet between 5 and 290 K. In view of the magnetic data, we propose a ...$D^{\bullet+}D^{\bullet+}A^{\bullet-}A^{\bullet-}D^{\bullet+}D^{\bullet+}A^{\bullet-}A^{\bullet-}$... linear chain structural motif. The $[DDQ]_2^{2-}$ dimer may act as a a diamagnetic buffer within these chains, thereby preventing any spin–spin interaction at low temperature. $[Fe(C_9Me_7)_2][TCNQ]$ has been structurally characterized as a linear chain salt consisting of alternating cations and anions stacked along a crystallographic axis. Magnetic data for this compound at 2 K suggest an intrachain spin alignment which can be modeled by the 1-D Heisenberg model with ferromagnetic interaction. We therefore suggest that the configurational interaction mechanism cannot provide a suitable explanation for the nature of the spin interactions in this compound. Further studies are required to assess the suitability of the recently proposed mechanism for ferromagnetic coupling in metallocenium charge-transfer salts, based on the spin polarization model proposed by Kahn *et al.*[11]

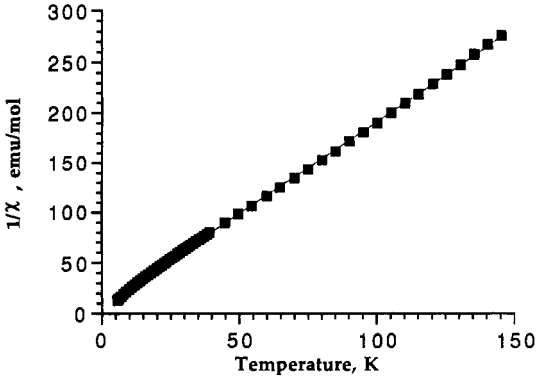

Figure 14. Plot of inverse molar susceptibility versus temperature for $[Fe(C_9Me_7)_2][DDQ]$.

Acknowledgment. We thank R. Scott Mclean for performing the Faraday measurements, M. Kurmoo for performing EPR measurements, and the SERC for financial support.

Supplementary Material Available: Tables giving crystallographic data and details of the structure determination, atom coordinates, bond lengths, bond angles, anisotropic thermal parameters, and least squares planes (10 pages). Ordering information is given on any current masthead page.